COMPARISON OF NUMERICAL AND ALGEBRAIC MODELS OF LOW AND HIGH PRESSURE HYDROGEN JET FLOWS WITH IDEAL AND REAL GAS MODELS

Xuefang Li, Jingliang Bi, David M. Christopher
Thermal Engineering Department
Key Laboratory for Thermal Science and Power Engineering of Ministry of Education
Tsinghua University
Beijing, China 100084

Abstract

Hydrogen transportation systems require very high pressure hydrogen storage containers to enable sufficient vehicle range for practical use. Current proposed designs have pressures up to 70 MPa with leakage due to damage or deterioration at such high pressures a great safety concern. Accurate models are needed to predict the flammability envelopes around such leaks which rapidly vary with time. This paper compares CFD predictions of jet flows for low pressure jets with predictions using the integral turbulent buoyant jet model. The results show that the CFD model predicts less entrainment and that the turbulent Schmidt number should be smaller, with 0.55 giving better results. Then, CFD predictions for very high pressure flows are compared with analytical models for choked flows that generate underexpanded jets into the ambient to evaluate the effects of the model assumptions and the effects of real exit geometries. Real gas effects are shown to accelerate the blowdown process and that real flow effects in the CFD model slow the flow rate and increase the exit temperature.

Keywords: Hydrogen jets, flammability envelopes, underexpanded jets, real gas flows

NOMENCLATURE

A	coefficient matrix in Eq. (9) and exit area (m^2)
b	hydrogen co-volume (m^3/kg) and characteristic jet size (m)
c	speed of sound (m/s)
const	constant in Eq. (12)
c_p	specific heat (J/kg K)
d_{H2}	hydrogen co-density (kg/m^3)
D_0	exit diameter (m)
D_{H2}	diffusivity of hydrogen in air (m^2/s)
E	entrainment (m^3/s)
Fr_{den}	density based Froude number
g	acceleration of gravity (m/s^2)
h	enthalpy (J/kg K)
j	time step number, diffusive mass flux (kg/m^2s)
m	mass in the tank (kg)
M	molecular weight of the mixture (kg/kg_{mol})
P	pressure (Pa)
Q	volumetric gas flow rate (kg/s)
r	jet radius (m)
R_g	ideal gas constant (J/kg K)
R	gas constant for the mixture (J/kg K)
S	distance along the jet centerline (m)
Sc_t	turbulent Schmidt number
t	time (s)
T	temperature (K)
u	velocity (m/s)
v	specific volume (m^3/kg)
V_0	exit velocity (m/s)

x distance in the horizontal direction (m)
y hydrogen mass fraction
y^+ dimensionless distance to the nearest wall in turbulence models
z compressibility and distance in the vertical direction (m)

Greek

Δt time step (s)
κ specific heat ratio
λ spreading ratio between the density and velocity fields
θ angle between the jet centerline and horizontal (°)
ρ density (kg/m^3)
μ_t turbulent viscosity (kg/ms)

Subscripts

0 exit
2 choked flow location
air air
cl centerline
cr critical pressure ratio for choked flow
H_2 hydrogen
i conditions inside the tank
∞ ambient

1.0 INTRODUCTION

Hydrogen is expected to play a strategic role in the energy mix of future low carbon societies according to the European Strategic Energy Technology Plan of the European Commission [1] and the Hydrogen, Fuel Cells & Infrastructure Technologies Program-Multi-Year Research, Development, and Demonstration Plan of the USA Department of Energy [2]. However, there are serious hydrogen safety issues that have to be fully addressed to demonstrate that hydrogen fuels can be widely used with the same or lower levels of risk as conventional fossil fuels. Fuel cells hold great promise for reducing our dependence on imported oil and for reducing pollution from vehicles. However, these fuels cells are expected to be powered by hydrogen which must be stored at high pressures in tanks at fueling stations and also in high pressure tanks in vehicles. Current plans anticipate pressures as high as 70 MPa for vehicles to have sufficient range for practical use. Since hydrogen is highly flammable, leaks from such tanks are of great concern to the public safety. Such leaks will result in high pressure jets flows into the surrounding atmosphere with the hydrogen mole fraction decreasing with distance from the leak. The lower hydrogen flammability limit in air is 4% by volume, so the location of the 4% mole fraction contour is of great importance. Hydrogen leaks have already lead to actual accidents causing much damage such as the accident in Stockholm, Sweden in 1983 involving the explosion of approximately 13.5 kg of hydrogen released from 200 bar working pressure tanks in a built up area of central Stockholm, Sweden. Venetsanos et al. [3] numerically simulated this hydrogen release and resulting explosion with the concentrations in the air and the combustion results giving reasonable qualitative agreement with the observed effects.

Hydrogen leakage from high pressure storage tanks will result in high pressure, underexpanded jets into the surrounding atmosphere. In this case, high pressures are those that result in choked flow at the exit with supersonic underexpanded jets outside the exit, while low pressure conditions do not result in choked flow at the exit and the resulting jet flow does not expand much in the atmosphere. Jets are also of importance in many other flow fields such as polluted or heated discharges into rivers, lakes or oceans, fuel jet flows into combustion chambers and exhaust plumes from chimneys. Hydrogen leaks are generally classified as low pressure, slow leaks where the jet if fully expanded leaving the orifice and as high pressure, underexpanded leaks where the flow leaving the orifice is choked and the jet expands greatly upon leaving the orifice. An integral similarity model has been widely used for low pressure leaks to predict the flow fields and pollutant distributions downstream of the leaks in many studies [4-13]. The older studies mainly focused on hot water discharges into rivers, lakes or oceans from industrial cooling systems. However, there has been renewed interest in this area due to the

present concerns about hydrogen leaks. Most of the experimental studies have used relatively small Froude numbers due to experimental size and cost limitations. Jets flows with Froude numbers greater than several hundred are considered to be momentum dominated flows where the jet momentum is most important and the buoyancy has little effect. Flows with smaller Froude numbers are referred to as buoyancy dominated flows where the buoyancy has a significant effect on both the jet trajectory and the entrainment. The integral model can also be used to predict the trajectories of buoyancy dominated flows, but the buoyancy introduces significantly more uncertainty into the predictions.
Computational fluid dynamics (CFD) methods are being widely used to assess these safety issues with numerous projects currently underway to evaluate and verify CFD model results. However, there are still numerous problems that have not been considered and numerous areas where experimental data is not available to validate the accuracy of CFD results. Thus, significant additional experimental and numerical studies are needed to increase the level of confidence in these theoretical and numerical models. [14].Numerical simulations typically use the Reynolds Averaged Navier Stokes (RANS) equations along with a variety of turbulence models. However, these turbulence models all have limitations for very complex flows involving significant turbulent mixing, laminar-turbulent interaction regions, and multiple component effects [15], all of which occur with high pressure hydrogen jets mixing with ambient air. Large Eddy Simulations and Direct Numerical Simulations have also been used, but they require much more computational time so they are not useful for practical applications.
Various conditions in the hydrogen-air cloud affect ignition such as the hydrogen concentration distribution within the cloud, the flow field and the turbulence within the cloud, so the flow conditions around the hydrogen jet and the spatial confinement of the hydrogen-air cloud both significantly affect the ignition conditions. As a result, computational models must be able to accurately predict the flow, temperature and concentration fields during the release and dispersion phases of an accident to accurately capture the ignition phase [14].
High pressure underexpanded hydrogen jets from a container will create very complex shock wave patterns around the nozzle exit with various types of shocks and expansion waves just outside the nozzle leading to a Mach disk where the jet flow velocity in the center of the jet slows to the local sonic velocity [16-18]. Accurately capturing these very complex flows requires very fine elements in a very large mesh. Investigations with comparisons to experimental data are needed to identify the level of detail necessary to correctly predict the shock structure to accurately describe the hydrogen dispersion in the far field.

1.1 CFD studies

There have been only a few numerical studies of high pressure highly under-expanded hydrogen jets into the atmosphere because the low density and high sonic speed of hydrogen make the numerical calculations very unstable [19]. Xu et al. [19] used a two-step approach based on the LES method to allow detailed mesh refinement in the sonic release region. They noted that there is no good experimental data available at such high source pressures for quantitative comparisons to validate their numerical results with only some quantitative comparisons possible, especially in the near release area. Angers et al. [20] did numerical simulations of hydrogen releases from a 70 MPa tank with verification based on the subsonic data of Swain [21]. They only presented results for very short times after initiation of the leak.
The complexities of CFD simulations have led to the development of the simplified notional nozzle concept using an effective Mach disk diameter [18, 22-25]. This approach does not specifically model the complex shock structure, but assumes that the release starts at the Mach disk (the location where the flow passes through a shock wave and becomes subsonic [16]). The notional nozzle diameter and flow velocity are estimated based on mass and momentum conservation between the exit and a point beyond the Mach disk where the pressure of the jet is equal to the ambient pressure. This notional nozzle approach has been widely used but involves some inaccuracies due to various assumptions, such as neglecting air entrainment into the jet and uncertainties in the temperature field [19]. However, Veser et al.[18] found that the approach gave good results for a tank pressure of 1.95 MPa. Tchouvelev [26] compared the notional nozzle approach with CFD calculations for a hydrogen release from a 43 MPa tank to show that the notional nozzle approach produced 25-30% longer flammable

clouds than the CFD model. Tchouvelevthen concluded that the main reason for this difference was the use of real gas properties in the actual leak approach while the notional nozzle approach used the ideal gas law. Thus, more modeling work is needed to improve the notional nozzle approach and to validate CFD models with experimental data at higher pressures. Han et al. [27] also found good results using a 2D steady-state, axisymmetric CFD model with the notional nozzle concept to predict the flow and concentration distributions for pressures up to 40 MPa.

In addition to the integral similarity model mentioned above, CFD models have also been used to model low pressure jet plumes, but such models also have limitations due to unknown constants in the model, such as the turbulent Schmidt number, which normally has the default value of $Sc_t = 0.7$, which can have a large effect on the results [28]. Velikorodny and Kudriakov [29] used an LES model to analyze the jet flow from a tank with an initial pressure of 30 MPa for air and helium discharges into air. They considered this a preliminary investigation of the near-field flow with future work to consider the far-field flow field. Khaksarfard and Paraschivoiu numerically predicted the jet dispersion for flows from an exit that was slowly increasing in size using the Noble-Abel EoS for only the initial several milliseconds of the release. Papanikolaou and Baraldi [30] compared the effects of various assumptions in four notional nozzle models on their predictive abilities using ideal gas properties. They also compared the abilities of various turbulence models in CFD models to predict the hydrogen dispersion for a 9.8 MPa tank pressure with the properties given by the Redlich Kwong equation of state.

Cheng et al. [31] compared numerically predicted release rates using the ideal gas and Noble-Abel equation of state [32] for a 40 MPa tank into air through a 6 mm diameter orifice to show that the real gas properties strongly affect the results with the ideal gas equation overestimating the release rates in the initial part of the discharge. They used a one-dimensional numerical model to predict the release rates using the TOPAZ code using both ideal gas and real gas properties [33] with PHOENICS to predict the plume after the release with both real and ideal gas properties.

1.2 Real gas effects

The properties of hydrogen and helium differ substantially from ideal gas predictions at high pressures and also at low temperatures that will occur as the jet expands into the atmosphere. For example, at an ambient temperature of 293 K and a pressure of 40 MPa, the hydrogen density is about 25% less than that predicted by the ideal gas law. The Noble-Abel equation of state, the NA-EOS, gives the compressibility, z, explicitly in terms inverse of the empirical hydrogen co-density, d_{H2} [32]:

$$z = \frac{P}{\rho R_g T} = (1-\rho b)^{-1} = 1 + \frac{bP}{R_g T} \tag{1}$$

where $b=1/d_{H2}$ for hydrogen is approximately 0.00775 m^3/kg, so the hydrogen co-density, d_{H2}, is about 129 kg/m^3.The hydrogen gas constant, R_g, is 4124 J/(kgK). The NA-EOS accounts for the finite volume of the gas molecules, but neglects the effects of intermolecular and cohesion forces. The compressibility predicted by the NA-EOS is compared with those given by the NIST data [34] in Fig. 1 where the lines are the NIST data and the symbols are the NA-EOS predictions. The EOS accurately predicts the compressibility reasonably well at higher temperatures and pressures, but not as well at low temperatures, where the compressibility is sometimes less than unity given by the ideal gas equation. This is near the two phase region where a crossover EoS may be more accurate; however, the crossover EoS are much more complex.

2.0 THEORETICAL MODELS

2.1 Low pressure integral jet model

The integral continuity, momentum and mass transport models have been used to predict the flow fields and pollutant distributions in many studies [4-13]. A typical buoyant jet geometry is shown in Fig. 2. The jet flow can be divided into the initial entrainment and heating zone, the flow development zone, the established flow zone and the decaying jet zone based on the flow development characteristics [13]. The first zone occurs for high pressure, low temperature jets where the

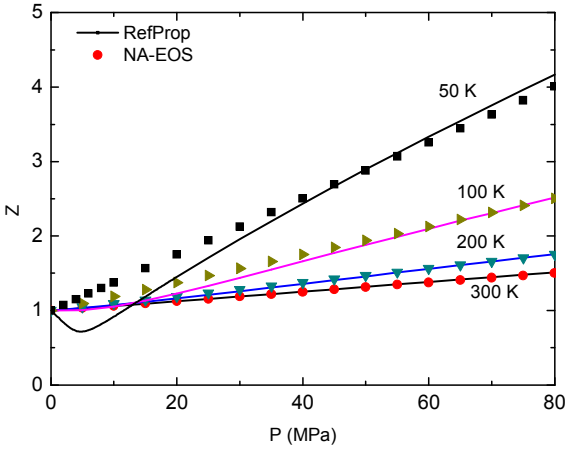

Figure 1. NA-EOS (symbols) and REFPROP [34] (lines) compressibilities of hydrogen.

entrainment into the jet results in a rapid temperature increase. Since the pressure was quite high, the flow at $s=S_0$ is still essentially a flat profile. In the flow development zone, the entrainment causes the flow profile to slowly change to a Gaussian profile but with the centerline velocity and concentration still the same as at the exit since entrained ambient fluid only diffusing exactly to the centerline at $s=S_E$. In the established flow zone, further entrainment causes the flow to gradually spread out as the centerline velocity and concentration decrease. This analysis of low pressure jets only considers the flow in the established flow zone with high pressure jets also including the first two zones. The model for the low pressure jets was based on the model used by Houf and Schefer[12] and Winter [13] which used a density based Froude number defined as:

$$\mathrm{Fr}_{den}=\frac{V_o}{\sqrt{gD_o\dfrac{(\rho_\infty-\rho_o)}{\rho_o}}} \tag{2}$$

Many experimental studies have shown that the density, velocity and concentration profiles can be approximated by Gaussian profiles for both momentum dominated and buoyancy dominated jets [7, 12, 36, 37]. The model results in a set of 4 differential equations with the distance along the centerline, S, as the independent variable. The continuity equation is [13]:

$$\left(b^2\rho_\infty-\frac{\lambda^2b^2}{\left(1+\lambda^2\right)}(\rho_\infty-\rho_{Cl}(S))\right)\frac{\partial}{\partial S}u_{Cl}(S)+u_{Cl}(S)\left(\rho_\infty-\frac{\lambda^2}{\left(1+\lambda^2\right)}(\rho_\infty-\rho_{Cl}(S))\right)2b\frac{\partial b}{\partial S}+ u_{Cl}(S)b^2\frac{\lambda^2}{\left(1+\lambda^2\right)}\frac{\partial}{\partial S}\rho_{Cl}(S)=\frac{\rho_\infty E}{\pi} \tag{3}$$

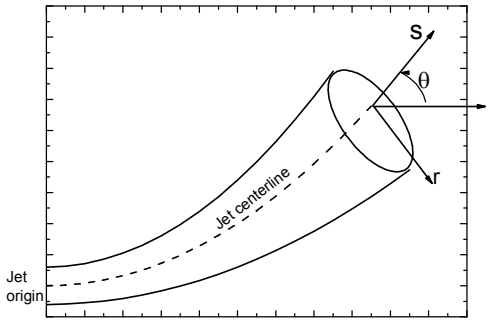

Figure 2. Buoyant jet geometry

The x momentum equation is:

$$\cos\theta\frac{b^2}{2}\rho_\infty\left[1-\frac{2\lambda^2}{\left(2\lambda^2+1\right)}\frac{(\rho_\infty-\rho_{Cl}(S))}{\rho_\infty}\right]2u_{cl}(S)\frac{\partial u_{cl}(S)}{\partial S}-(\sin\theta)u_{cl}^2(S)\frac{b^2}{2}\rho_\infty\left[1-\frac{2\lambda^2}{\left(2\lambda^2+1\right)}\frac{(\rho_\infty-\rho_{Cl}(S))}{\rho_\infty}\right]\frac{\partial\theta}{\partial S}+$$
$$u_{cl}^2(S)\cos\theta\rho_\infty\left[1-\frac{2\lambda^2}{\left(2\lambda^2+1\right)}\frac{(\rho_\infty-\rho_{Cl}(S))}{\rho_\infty}\right]b\frac{\partial b}{\partial S}+u_{cl}^2(S)(\cos\theta)\frac{b^2}{2}\frac{2\lambda^2}{\left(2\lambda^2+1\right)}\frac{\partial\rho_{Cl}(S)}{\partial S}=0 \quad (4)$$

The z momentum equation is:

$$\sin\theta\frac{b^2}{2}\rho_\infty\left[1-\frac{2\lambda^2}{\left(2\lambda^2+1\right)}\frac{(\rho_\infty-\rho_{Cl}(S))}{\rho_\infty}\right]2u_{cl}(S)\frac{\partial u_{cl}(S)}{\partial S}+u_{cl}^2(S)\cos\theta\frac{b^2}{2}\rho_\infty\left[1-\frac{2\lambda^2}{\left(2\lambda^2+1\right)}\frac{(\rho_\infty-\rho_{Cl}(S))}{\rho_\infty}\right]\frac{\partial\theta}{\partial S}$$
$$+u_{cl}^2(S)\sin\theta\rho_\infty\left[1-\frac{2\lambda^2}{\left(2\lambda^2+1\right)}\frac{(\rho_\infty-\rho_{Cl}(S))}{\rho_\infty}\right]b\frac{\partial b}{\partial S}+u_{cl}^2(S)\sin\theta\frac{b^2}{2}\frac{2\lambda^2}{\left(2\lambda^2+1\right)}\frac{\partial\rho_{Cl}(S)}{\partial S}=(\rho_\infty-\rho_{Cl}(S))g\lambda^2b^2 \quad (5)$$

The species concentration is:

$$\left(-\rho_{Cl}(S)y_{Cl}(S)\frac{\left(1+\lambda^2\right)b^2}{2}\right)\frac{\partial u_{Cl}(S)}{\partial S}+\left(-u_{Cl}(S)y_{Cl}(S)\frac{\left(1+\lambda^2\right)b^2}{2}\right)\frac{\partial\rho_{Cl}(S)}{\partial S}+\left(-u_{Cl}(S)\rho_{Cl}(S)\frac{\left(1+\lambda^2\right)b^2}{2}\right)\frac{\partial y_{Cl}(S)}{\partial S}+$$
$$+\left(-u_{Cl}(S)y_{Cl}(S)\rho_{Cl}(S)\frac{\left(1+\lambda^2\right)}{2}\right)2b\frac{\partial b}{\partial S}+\left[y_\infty\left\{\rho_\infty\frac{b^2}{2}-(\rho_\infty-\rho_{Cl}(S))\frac{\lambda^2b^2}{2\left(1+\lambda^2\right)}\right\}\right]\frac{\partial u_{Cl}(S)}{\partial S}+ \quad (6)$$
$$\left[u_{Cl}(S)y_\infty\left\{\rho_\infty-(\rho_\infty-\rho_{Cl}(S))\frac{\lambda^2}{\left(1+\lambda^2\right)}\right\}\right]b\frac{\partial b}{\partial S}+\left[u_{Cl}(S)y_\infty\frac{\lambda^2b^2}{2\left(1+\lambda^2\right)}\right]\frac{\partial\rho_{Cl}(S)}{\partial S}=0$$

These can be solved for the derivatives of the centerline velocity, u_{Cl}, the jet angle, θ, the centerline density, ρ_{Cl}, and the characteristic jet width, b, as functions of the position along the jet centerline, S. The species concentration is also not known, but is related to the density through the ideal gas equation:

$$P=\rho_{cl}(S)R(S)T=\rho_{cl}(S)\frac{R_g}{M}T \quad (7)$$

Where P is assumed to be 101.3 Pa (1 atm) and T is assumed to be constant at the ambient temperature. The molecular weight of the mixture is then related to the mass fraction, y_{Cl}, as:

$$\frac{1}{M}=\frac{y_{cl}(S)}{M_{H_2}}+\frac{1-y_{cl}(S)}{M_{air}} \quad (8)$$

The derivative of the centerline species concentration in Eq. (8) with respect to S was then substituted into Eq. (6). Equations (3) – (6) were then solved as a set of linear equations for the derivatives after writing in matrix form (with $y_\infty = 0$) as:

$$[A]\begin{bmatrix}\frac{du_{Cl}}{dS}\\ \frac{db}{dS}\\ \frac{d\theta}{dS}\\ \frac{d\rho_{Cl}}{dS}\end{bmatrix}=\begin{bmatrix}\frac{\rho_\infty E}{\pi}\\ 0\\ (\rho_\infty-\rho_{Cl}(S))g\lambda^2b^2\\ 0\end{bmatrix} \quad (9)$$

Where the entries in matrix [A] are the coefficients from Eqs. (3) – (6). Equation (9) was solved along with the differential equations for the jet coordinates to calculate the jet trajectory and the species concentration decay. Attempts to solve for the derivative of the centerline species concentration in Eq. (8) using the results of the previous time step in Eq. (6) were not successful since the result is very sensitive to the coefficients. The initial conditions used for the solution of the integral model equations were the initial centerline velocity determined from the given Froude number defined in Eq.

(2), the initial value of θ given by the geometry, the initial centerline density for pure hydrogen at 295 K, an initial centerline hydrogen mass concentration of 1, an initial location of (0,0) and an initial jet diameter.

2.2 High pressure blowdown model

The blowdown of a very high pressure tank can be modeled as an isentropic expansion inside the tank with isentropic flow from the tank to the nozzle exit. Thus, the pressures and temperatures in the tank can be predicted using the isentropic expansion equations. The expansion was modeled using the ideal gas equations and the Noble-Abel EoS in Eq. (1) which can be rewritten as:

$$p(v-b)=R_gT \tag{10}$$

The ideal gas equation simply has b=0, so the following model also applies to an ideal gas when b is set equal to zero. The velocity at the exit, location 2, is given by:

$$u_2=\sqrt{2(h_i-h_2)}=\sqrt{2c_p(T_i-T_2)} \tag{11}$$

where the specific heat is given by $c_p=\kappa R_g/(\kappa\text{-}1)$ where $\kappa$is the ratio of the specific heats. The first part of the equation is due for any gas, while the second part is only true for gas models where the enthalpy can be related to the specific heat and the temperature. The p-v relationship for an isentropic expansion of a Noble-Abel gas is given by [35]:

$$p(v-b)^{\kappa}=const \tag{12}$$

Combining Eqs. (10) – (12) gives:

$$u_2=\sqrt{\frac{2\kappa}{\kappa-1}p_i(v_i-b)\left(1-\left(\frac{p_2}{p_i}\right)^{\frac{\kappa-1}{\kappa}}\right)} \tag{13}$$

where the subscript i indicates the conditions inside the tank. For supersonic flow, the flow at the exit when choked, which is the speed of sound, is given by [35]:

$$c_2=\frac{v_2}{v_2-b}\sqrt{\kappa R_gT_2} \tag{14}$$

The critical pressure ratio for choked flow is then:

$$v_{cr}=\frac{p_2}{p_i}=\left(1+\frac{\kappa-1}{2}\left(\frac{v_2}{v_2-b}\right)\right)^{\frac{\kappa}{1-\kappa}} \tag{15}$$

Thus, if the flow is choked, the exit pressure (location 2) is the critical pressure ratio times the upstream pressure, but is equal to the ambient pressure if not choked:

$$p_2=\begin{cases}p_iv_{cr} & (p_iv_{cr}>p_\infty)\\ p_\infty & (p_iv_{cr}\le p_\infty)\end{cases} \tag{16}$$

The gas flow rate at the exit is then:

$$Q=\frac{Ac_2}{v_2} \tag{17}$$

Taking the derivative of Eq. (12) gives a relationship between the pressure change and the specific volume change for an isentropic expansion as:

$$\frac{dp_i}{p_i}=-\kappa\frac{dv_i}{v_i-b} \tag{18}$$

The rate of change of the mass in the tank is then given by:

$$dm_i=-Qdt \tag{19}$$

where dt is the time step. Equations (17) – (19) can then be combined to relate the mass in the tank to the specific volume change:

$$\frac{dm_i}{m_i} = -\frac{Qdt}{m_i} = -\frac{dv_i}{v_i} \tag{20}$$

Equations (13) and (15) – (20) can then be combined to give the change in the specific volume and the pressure in the tank as a function of the flow rate and the time where j indicates the time step and Δt indicates the time step size:

$$v_i^{(j+1)} = v_i^{(j)}\left(1+\frac{Q^{(j)}}{m_i^{(j)}}\Delta t\right) \tag{21}$$

$$p_i^{(j+1)} = p_i^{(j)}\left(1-\kappa\frac{v_i^{(j+1)}-v_i^{(j)}}{v_i^{(j)}-b}\right) \tag{22}$$

The flow rates, the exit pressure and the conditions inside the tank can then be calculated during the blowdown for either an ideal gas or a Noble-Abel gas.

2.3 Numerical jet models

The jet trajectory and species concentrations were also modeled by solving the Navier-Stokes equations for turbulent flow with mass transfer for both low pressure jets and high pressure, underexpanded jets. The low pressure flow was modeled using both 2D and 3D models. The 2D assumed the flow to be axisymmetric with the flow modeled by solving the two-dimensional, axisymmetric Navier-Stokes equations with the k-ω low Reynolds number turbulence model and the species transport equation:

$$\nabla\cdot(\rho\vec{v}y_{H_2}) = \nabla\cdot(\rho D_{H_2}+\frac{\mu_t}{Sc_t})\nabla y_{H_2} \tag{23}$$

Where μ_t is the turbulent viscosity given by the turbulence model and Sc_t is the turbulent Schmidt number. The blowdown process and the jets were also modeled by solving the same equations in a three dimensional geometry. The y^+ along the tube wall were all less than 2 for the k-ω turbulence model. The viscosity was calculated using the ideal gas mixing law; although, this had little effect. The diffusion coefficient was calculated using the kinetic theory model in Fluent, but this had only a small effect near the orifice since the diffusion coefficient is almost constant for hydrogen mass ratios less than 50%. The tube wall roughness also had little effect on the jet profile. The 2D axisymmetric mesh had 82,000 cells with the cells concentrated near the jet exit in both the axial and radial directions and near the wall. The 3D model was found to be more stable with the k-ε turbulence model since the elements near the wall could not be as small for a 3D transient calculation as in the

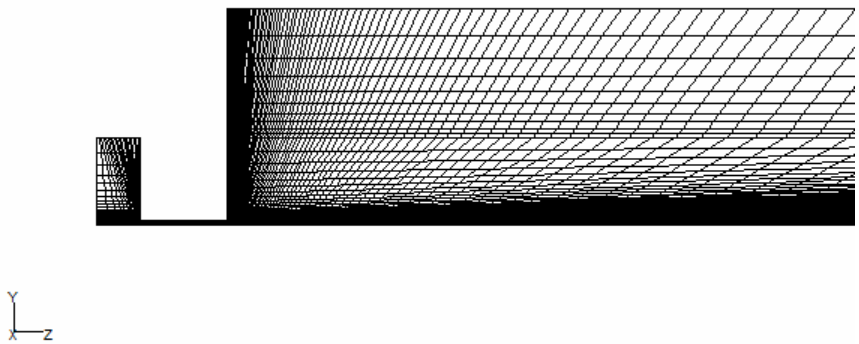

Figure 3. 3D mesh for the high pressure jet simulations with 101,000 elements.

2D model with the mesh having over 101,000 elements with a cylindrical region with hexahedral elements throughout the entire region with the elements concentrated near the jet orifice in all three directions. 3D calculations with 196,000 elements resulted in blowdown times that were about 5% slower depending on the numerical parameters (time step, convergence factors, and number of iterations). The smaller 3D mesh was then used to reduce the computational times even on a parallel computer. Besides the number of elements, the element sizes in critical locations, such as along the wall and in the shock wave regions, also strongly affected the calculational accuracy and the convergence.

The high pressure CFD model used a 3D model after the 2D axisymmetric model was found to not give reasonable results. The high pressure model was used to analyze a transient blowdown of a 4 L tank through the 2 mm diameter exit at the end of a 20 mm long, 2 mm diameter tube. The mesh shown in Fig. 3 was carefully constructed so that it contained all hexahedral elements after tetrahedral elements were found to cause divergence. The tank on the left in Fig. 3, the tube in the middle and the air region on the right were all quarter cylinders with an o-grid used in the middle to get all hexahedrals. The air region was 700 mm long with a radius of 50 mm. The model included a small tank as part of a virtual 4 L tank which simulated the conditions for a blowdown of a large tank. The inlet pressure and temperature for the tank region of the mesh on the left were calculated based on the isentropic equations:

$$\frac{P_i(t)}{P_i(0)} = \left(\frac{\rho_i(t)}{\rho_i(0)} \right)^{\kappa} \qquad \text{and} \qquad \frac{T_i(t)}{T_i(0)} = \left(\frac{\rho_i(t)}{\rho_i(0)} \right)^{\kappa-1} \tag{24}$$

where the subscript i indicates the conditions in the virtual tank. The density in the tank was calculated from the virtual tank volume and the mass remaining in the tank which was calculated using Eq. (19). The tank was then connected to the air region by the 2 mm diameter tube. The flow rate was calculated by Fluent at the entrance to the tube. The flow was assumed to be symmetric so only one fourth of the geometry was modeled. The boundary condition on the outer surface of the air was a pressure inlet with the right end being a pressure outlet. Calculations with the mesh having 101,000 elements were done with various times steps with a time step of 0.004 s giving reliable results for a reasonable calculational times. Under relaxation factors of 0.1 to 0.6 gave very similar results. The calculations used the density solver in Fluent with the standard k-ε turbulence model with the non-equilibrium boundary conditions (the standard boundary conditions gave similar results). The transport equations were all discretized using the Fluent second-order central difference model.

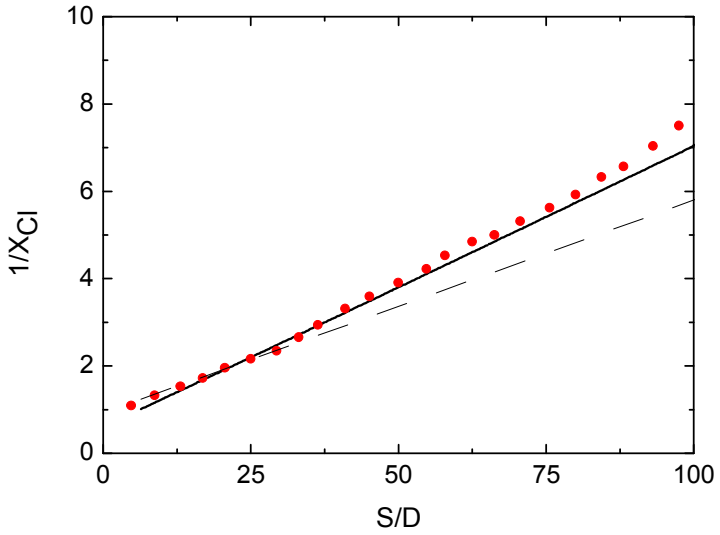

Figure 4. Comparison of the centerline concentration decay (mole fraction) predicted by the integral model (solid line) with experimental data [12] and the correlation of Chen and Rodi [38] (dashed line) for a vertical jet with Fr_{den}=268 and exit diameter of 1.9 mm.

3.0 Results:

3.1 Integral model:

The integral model was verified by solving for a vertical jet for comparison with experimental results. The model calculated the centerline location, velocity and concentration and the characteristic jet width. The centerline concentration and the characteristic jet width were then used with the assumed Gaussian concentration profile that has been found to accurately represent experimental measurements [12, 13, 35, 36, 37, 38] to calculate the locations of the 4% mole fraction profiles. The results for a Froude number of 268 and an exit diameter of 1.9 mm show that the hydrogen concentration falls below the lower flammability limit about 0.7 m from the exit and that the flammability region has a jet width of several centimeters for a vertical jet. The decay in the centerline hydrogen molar concentration ratio with distance from the exit is compared with measured experimental data [12] in Fig. 4 where D is the exit diameter. The results agree very well for this vertical jet with the differences increasing for S/D~100 due to more entrainment into the jet than given by the model which further reduces the molar concentration ratio. Chen and Rodi [40] analyzed a large amount of data to develop a similarity law for the concentration delay in expanded jets:

$$\frac{y_{cl}(x)}{y(0)} = 5.4\sqrt{\frac{\rho(0)}{\rho_\infty}}\frac{D_0}{x} \tag{25}$$

where y(0) is the mass fraction at the nozzle and ρ(0) is the hydrogen density at the nozzle. Molkov[41] then surveyed a large amount of data to confirm this similarity law for both expanded and under-expanded jets. Equation (25) overpredicts the concentrations farther from the exit by about the same amount as can be seen in the data in Molkov [41].

Typical 4% flammability envelopes for horizontal jets are shown in Fig. 5. Figure 5 shows that the jet for Fr_{den}=500 is almost completely momentum dominated with the centerline only rising about 20 cm at the end of the flammability envelope. The maximum length of the flammability envelope for jets in both the horizontal and vertical directions predicted by the integral model are proportional to the orifice diameter so the envelopes in Fig. 5 are much larger than for smaller orifice diameters. The flammability envelope profiles for the smaller Froude numbers show the strong influence of buoyancy on the envelope profile with the envelope for Fr_{den}=40 extending out less than 60 cm but quickly rising.

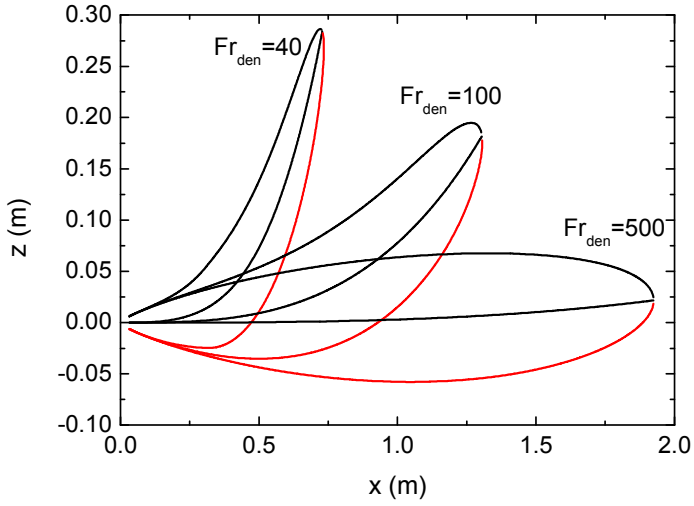

Figure 5. Flammability envelopes for horizontal jets from a 5 mm diameter orifice.

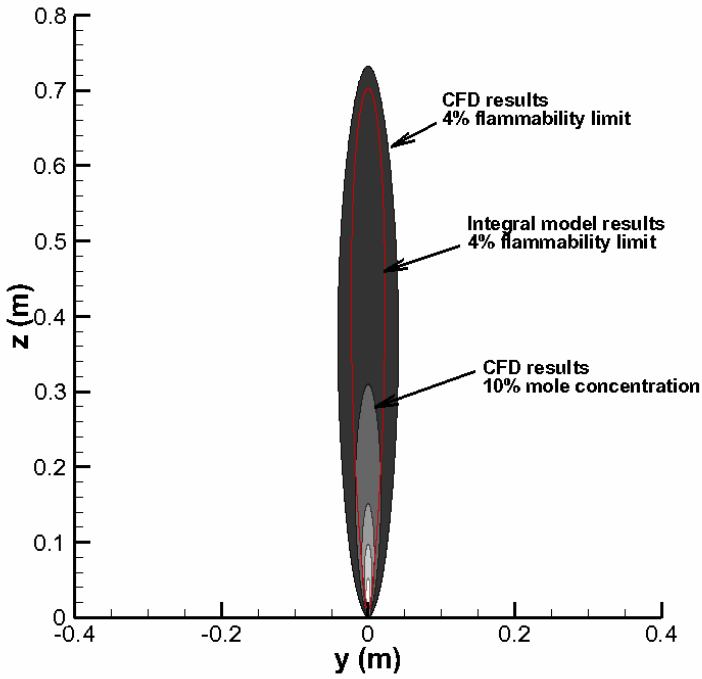

Figure 6. Comparison of CFD and integral model results for Fr_{den}=268 and an orifice diameter of 1.905 mm

3.2 Low pressure Navier-Stokes model

The CFD model was also used to predict the jet profiles for a variety of conditions for both 2D axisymmetric and 3D jets. The jet profile predict by the CFD model is compared with the integral model results in Fig. 6 for a vertical jet with Fr_{den}=268 and an orifice diameter of 1.905 mm. The 4% flammability envelope predicted by the CFD model is slightly larger than that predicted by the integral model which suggests that the CFD model includes somewhat less entrainment than the integral model. The results in Fig. 6 also show the region with the 4% molar concentration is much larger than with the 10% molar concentration due to the significant entrainment of air into the hydrogen stream. The centerline molar concentration profiles predicted by the 2D and 3D models are compared with the experimental data in Fig. 7. The default turbulent Schmidt number used in Fluent of Sc_t = 0.7 is known to have a large effect on the diffusion results [28]. The results for the default value for the 2D axisymmetric Fluent model are seen in Fig. 7 to be well below the experimental data while the results for the 3D Fluent model are higher than the 2D results, but still below the experimental data. Decreasing the turbulent Schmidt number to 0.55 yields numerical predictions that are in good agreement with the experimental data, especially for z/D less than 90 where buoyancy has little effect. Decreasing the turbulent Schmidt number increases the turbulent contribution to the diffusion. In Fig. 7, the inverse of the concentration predicted by the CFD model being lower than the experimental data is consistent with the observations in Fig. 6 that the concentrations predicted by the CFD model are higher. A smaller turbulent Schmidt number will increase the turbulent diffusion since the mass diffusion flux is given by:

$$j = -(\rho D_{H2} + \frac{\mu_t}{Sc_t})\Delta y \tag{26}$$

The 2D and 3D CFD results in Fig. 7 also both illustrate that the length of the flow development zone given by the numerical results agrees well with the frequently cited empirical value given by Abraham [8] of S/D=6.2.

The centerline velocities predicted by the CFD model for a vertical jet with Fr_{den}=268 are compared with the centerline velocities predicted by the integral model in Fig. 8. The initial centerline velocity given by the CFD model is much higher than that given by the integral model (which is the same as the average value given by Houf and Schefer [12]) because the CFD model includes the flow development along the inlet tube (as in the experiment) while the integral model starts from the

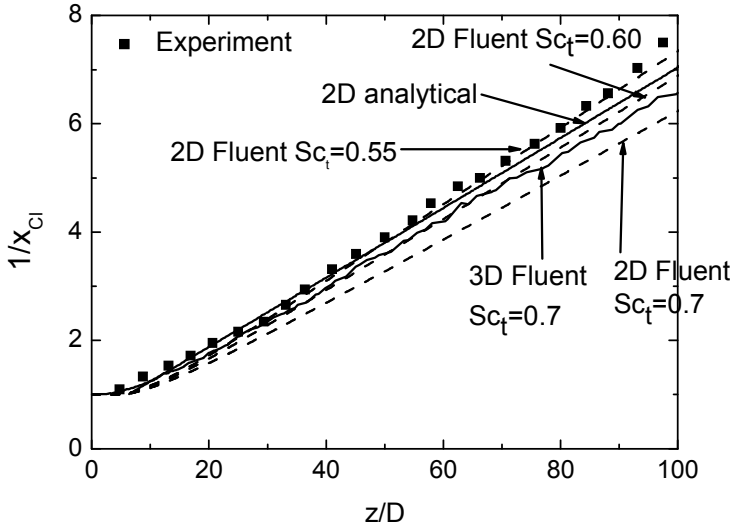

Figure 7. Centerline molar concentration ratios predicted by the 2D (dashed lines) and 3D models Fr_{den}=268.

average velocity. For fully developed flow in a circular tube, the centerline velocity would be twice the average velocity, but the flow in the tube is far from fully developed with L/D Re ~ 0.004, so the centerline velocity is still somewhat less than twice the average.

While the integral model is useful for quickly predicting the velocity and concentration distributions as well as the flammability envelopes, they cannot be applied to confined jets where the jet flow impinges on some obstacle. CFD models are needed for such confined jets to accurately predict the flammability envelopes. CFD models are also needed to predict transient results, especially for high pressure jets where the transient conditions are more important. Thus, better models are needed to predict the flow development within hydrogen jets, especially for interactions of the jet with nearby structures. In addition, there are no known studies that provide measurements of the jet velocities, so experimental measurements of jet velocities are needed to improve and verify these models.

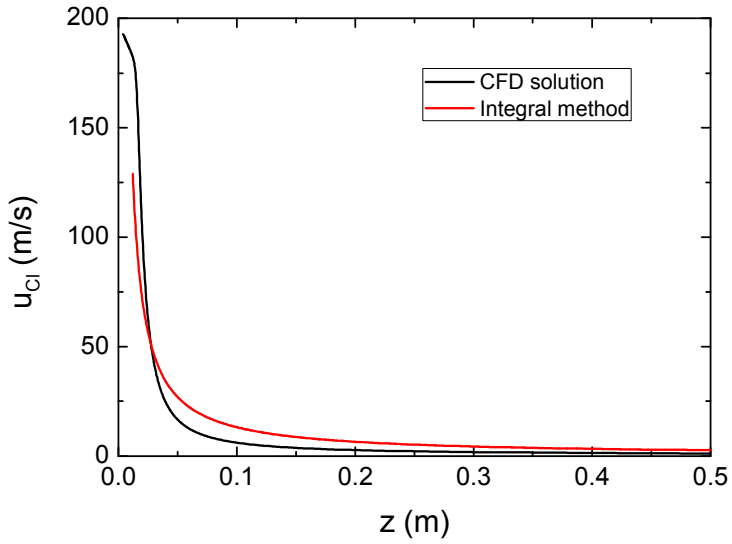

Figure 8. Centerline velocities predicted by the CFD and integral models for Fr_{den}=268 and a 1.905 mm diameter orifice.

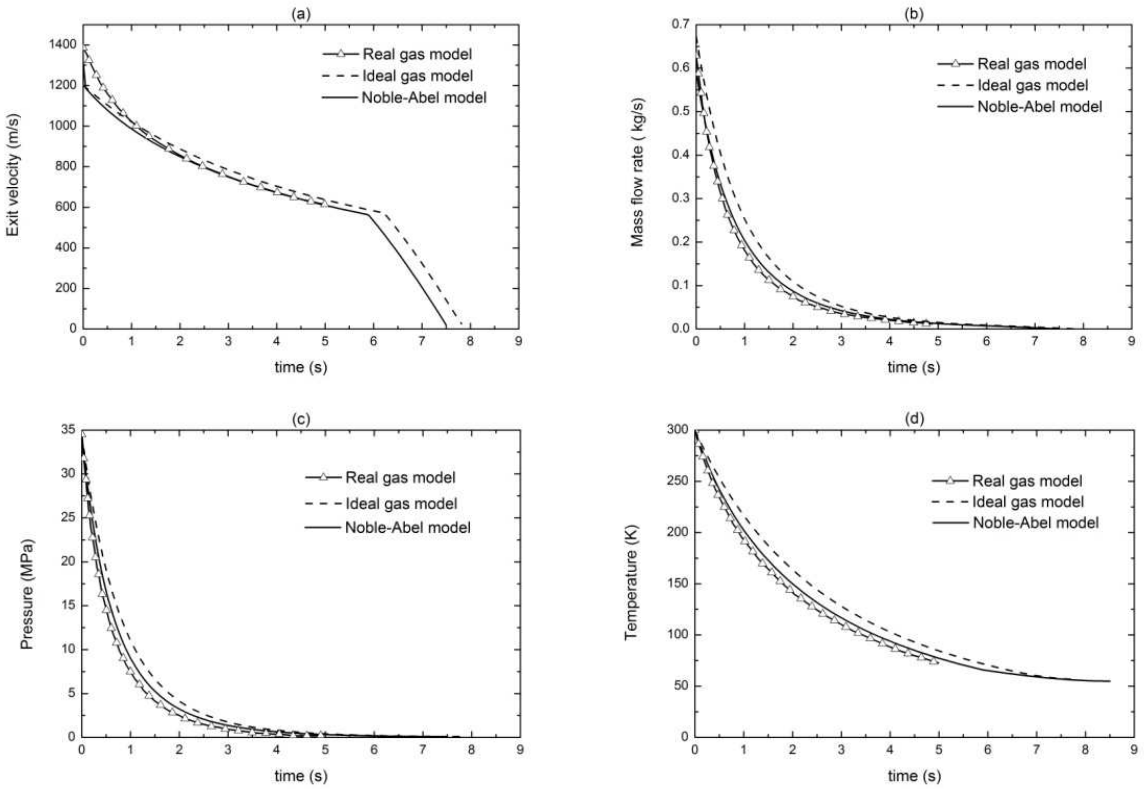

Figure 9. Hydrogen release conditions for flow from a tank at an initial pressure of 34.5 MPa and an initial temperature of 300 K for the ideal-gas model, Noble-Abel model and the real gas model given by Mohamed and Paraschivoiu [40]. (a) Exit stream velocity, (b) mass flow rate, (c) stagnation pressure inside the tank and (d) stagnation temperature.

3.3 High pressure blowdown model:

The high pressure blowdown model given by Eqs. (10) – (22) was solved for an initial tank pressure of 34.5 MPa and an initial tank temperature of 300 K using the ideal gas model and the Noble-Abel EoS with comparison to the results of Mohamed and Paraschivoiu [42] who used the Beattie-Bridgeman equation of state to predict the properties. These conditions would give a highly superheated vapor in the tank. The results shown in Fig. 9 shown the predicted exit velocity, flow rate, and the tank stagnation pressure and temperature. The initial exit velocity is higher for the real gas model but it quickly decreases to the same value as for the Noble-Abel model. The ideal gas model predicts higher exit velocities for most of the blowdown with a slightly later bend in the curve where the flow is no longer choked. The mass flow rates are also higher for the ideal gas model. The tank pressures and temperatures predicted by the real gas model are both slightly lower than those predicted by the Noble-Abel model which are somewhat lower than the ideal gas model results. The ideal gas model has higher exit velocities and flow rates, but still has a longer blowdown time because the ideal gas model initially has a greater amount of hydrogen in the tank as shown in Table 1. Since

Table 1. Initial hydrogen masses and hydrogen compressibilities and the total leak times predicted by the ideal-gas model, Noble-Able model and the real gas model by Mohamed and Paraschivoiu [42] for an initial pressure of 34.5 MPa.

	Initial Mass (kg)	Compressibility, Z	Total time (s)
	34.5 MPa	34.5 MPa	34.5 MPa
Ideal gas model	0.761	1.0	7.8
Noble-Abel model	0.627	1.21	7.5
Real gas model	0.576	1.32	—

the density is inversely proportional to the compressibility as shown in Eq. (1), a larger compressibility will result in a smaller density and less mass in the tank at the beginning of the blowdown process. The difference becomes more pronounced at higher pressures. The results in Fig. 9 also show that the tank temperature decreases greatly during the blowdown with the final value approaching the critical temperature, which is 33 K for hydrogen. The exit temperature after the isentropic expansion into the exit would be even lower.

3.4 High Pressure jet model

High pressure jets were also modeled by solving the Navier-Stokes equations for an initial tank pressure of 70 MPA and an initial tank temperature of 300 K during the blowdown of a 4 L tank through a 2 mm diameter hole. The tank pressure histories are shown in Fig. 10. Fluent using ideal gas properties predicts the slowest blowdown because the model has additional flow resistance in the exit tube that is not considered in the three algebraic models. The ideal gas model is again slower because it initially has a greater amount of hydrogen in the tank and because the sonic velocities for the ideal gas are less than for the Noble-Abel model. The Noble-Abel model is a little faster with the model using the RefProp properties giving the fastest blowdown. The predicted temperatures at the exit are shown in Fig. 11. The Fluent result is at a point in the middle of the exit tube, while the algebraic model is for an ideal exit geometry, so the geometries differ. The exit temperature predicted by Fluent initially increases some as the gas in the exit tube is compressed by the high pressure gas exiting the tank. The temperatures in both models then very rapidly decrease due to the isentropic expansion of the gas in the tank as the pressure decreases and due to the isentropic expansion of the fluid accelerating to the exit. The exit temperature predicted by Fluent initially decreases much more and then recovers, possibly due to the shock waves forming in the tube and then at the tube exit. The temperature calculation for the algebraic model stopped at 11 s when the flow was no longer choked. The exit temperatures predicted by Fluent are higher than those predicted by the algebraic model for most of the blowdown process most likely due to the non-ideal characteristics of the flow, especially the real flow effects of the flow passing through the short tube that are not considered in the algebraic model. However, the temperatures at the end of the choked flow periods are similar.

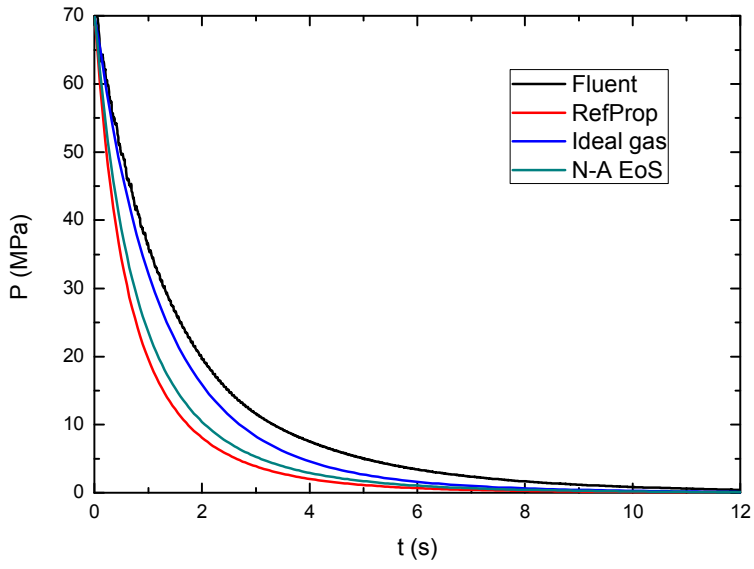

Figure 10. Pressure histories during the blowdown of a 4 L tank through a 2 mm diameter hole using the high pressure Fluent model and the ideal gas, Noble-Abel and RefProp models.

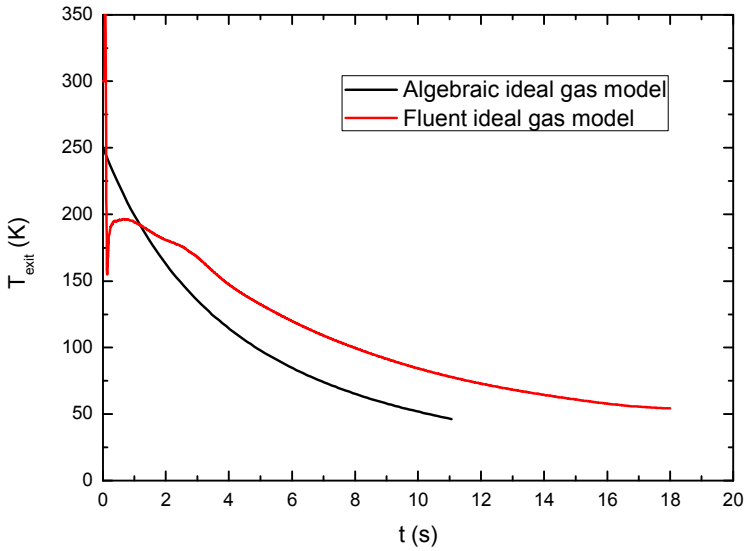

Figure 11. Exit temperatures during for ideal gas properties for a blowdown from 70 MPa.

The hydrogen molar species concentration histories are shown in Fig. 12 at four locations 50, 100, 200 and 300 tube diameters from the tube exit, with all four on the centerline. The hydrogen concentrations at all four locations increase very rapidly as the jet reaches each point with only the point 50d from the exit having almost pure hydrogen. All four locations have exceeded the lower flammability limit of 4%, but are quickly decreasing as the hydrogen diffuses into the atmosphere and the flow from the tank slows. A typical Mach disk profile is shown in Fig. 13 during the blowdown with supersonic flow between the exit and the Mach disk and a partially formed barrel shock around the flow downstream of the Mach disk.

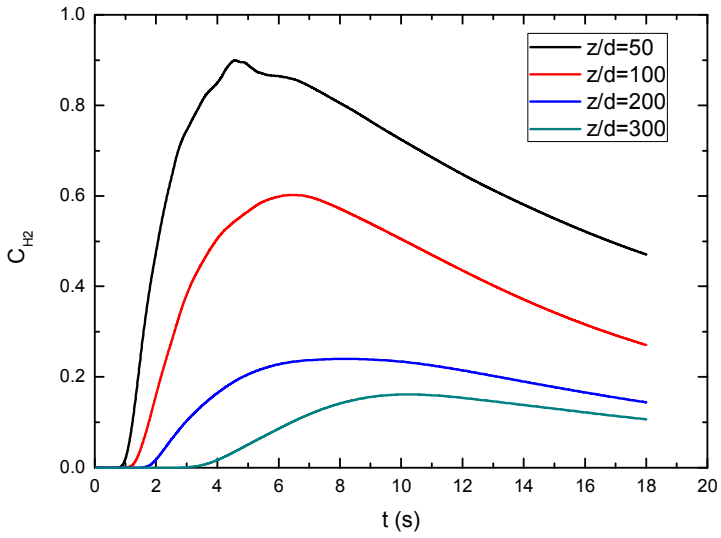

Figure 12. Hydrogen molar species concentrations predicted by the CFD model using the ideal gas model at four locations in the jet region for an initial tank pressure of 70 MPa.

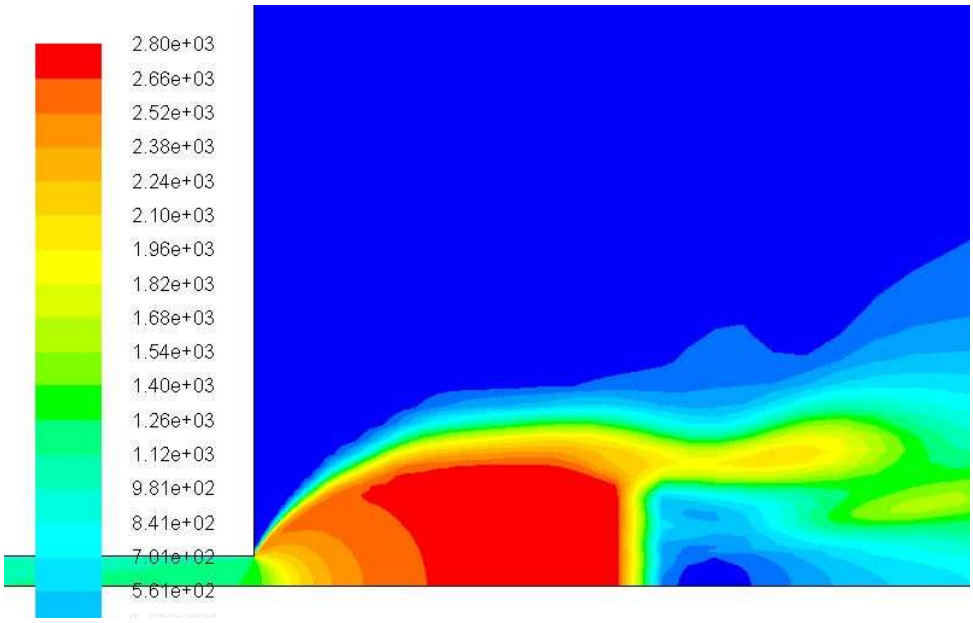

Figure 13 Velocities in the Mach disk region for a 70 MPa blowdown.

4.0 CONCLUSIONS

This study compares predictions of the jets created by low pressure and high pressure hydrogen escaping from small leaks in storage tanks. The low pressure flows are modeled using the integral model for jets that satisfy the similarity criteria with both low and high pressure flows modeled using CFD models. This study then also compares predictions of the tank pressure and temperature for high pressure leaks as a hydrogen storage tank empties. The high pressure models are used to compare the effects of ideal versus real gas models and the predictions of ideal isentropic flow models with CFD predictions.

Comparison of the low pressure results with experimental data shows that the CFD models predict less entrainment than the integral model. The results further indicate that the default turbulent Schmidt number of 0.7 in Fluent should be reduced some to about 0.55 since the turbulent Schmidt number has a large effect on the entrainment into the jet. The applicability of this conclusion to high pressure jets effects needs to be further verified by comparisons of CFD models with high pressure experimental data.

The high pressure models show that the blowdown times for the ideal and real gas models differ with the real gas models having faster blowdown times because the ideal gas model initially has a larger amount of hydrogen in the tank and the speed of sound for the ideal gas model is less than the speed of sound for the real gas models, which affects the flow rate exiting the tank since most of the process is choked. The results also show that real flow effects increase the temperatures leaving the tank even for an ideal gas model, but that the temperatures at the end of the choked flow period are similar.

Acknowledgement:
This work was supported by the National Basic Research Program of China ("973" Project), Grant No. 2011CB706904.

References:

1. EC, 2007. Communication from the Commission: A European strategic energy technology plan (SET-Plan) - Towards a low carbon future, Brussels, 22 November 2007, COM (2007) 723 final.
2. DoE, 2007. Hydrogen, Fuel Cells & Infrastructure Technologies Program-Multi-Year Research, Development, and Demonstration Plan. Planned program activities for 2005-2015.

3. Venetsanos, A.G., Huld, T., Adams, P., Bartzis, J.G., Source, dispersion and combustion modeling of an accidental release of hydrogen in an urban environment, Journal of Hazardous Materials, **A105**, 2003, pp. 1-25.
4. Gebhart, B., Hilder, D.S., Kelleher, M., The diffusion of turbulent buoyant jets, Advances in Heat Transfer, New York: Academic Press, 1984, **16**.
5. Hirst, E.A. Analysis of buoyant jets within the zone of flow establishment. Oak Ridge National Laboratory, Report ORNLTM-3470, 1971.
6. Albertson, M.L., Dai, Y.B., Jensen, R.A., Rouse, H., Diffusion of submerged jets, Transactions of the American Society of Civil Engineers, **115**, 1950, pp. 639-697.
7. Morton, B.R., Taylor, G.I., Turner, J.S., Turbulent gravitational convection from maintained and instantaneous sources. Proceedings of the Royal Society of London, Ser. **A234**, 1956, pp. 1-23.
8. Abraham, G., Horizontal jets in stagnant fluid of other density, Journal of the Hydraulic Division of the American Society of Civil Engineers, **9**, 1965, pp. 139-154.
9. List, E.J., Imberger, J., Turbulent entrainment in buoyant jets and plumes, Journal of the Hydraulic Division of the American Society of Civil Engineers, **99**, 1971, pp. 1461-1474.
10. Riester, J.B., Bajura, R.A., Schwartz, S.H., Effects of water temperature and salt concentration on the characteristics of horizontal buoyant submerged jets, Journal of Heat Transfer, **102**, 1980, pp. 557-562.
11. Davis, L.R. Shirazi, M.A., Slegel, D.L., Measurement of buoyant jet entrainment from single and multiple sources, Journal of Heat Transfer, **100**, 1978, pp. 442-447.
12. Houf, W., Schefer, R.W., Analytical and experimental investigation of small-scale unintended releases of hydrogen, International Journal of Hydrogen Energy, **33**, 2008, pp. 1435 – 1444.
13. Winter, W.S., Modeling Leaks from Liquid Hydrogen Storage Systems, Sandia National Laboratory, Report SAND2009-0035, 2009.
14. Baraldi, D., Papanikolaou, E., Heitsch, M., Moretto, P., Cant, R. S., Roekaerts, D., Dorofeev, S., Koutchourko, A., Middha, P., Tchouvelev, A.V., Ledin, S., Wen, J., Venetsanos, A., Molkov, V.V., Gap Analysis of CFD Modelling of Accidental Hydrogen Release and Combustion, JRC Scientific and Technical Report, European Commission Joint Research Centre Institute for Energy, 2010.
15. Hirsch C., Tartanville B., Reynolds Averaged Navier-Stokes modeling for industrial applications and some challenging issues. International Journal of Computational Fluid Dynamics, **23**, 2009, pp. 295-303.
16. Crist, S., Sherman, P.M., Glass, R.R., Study of highly underexpanded sonic jet, AIAA Journal, **4**, No. 1, 1966, pp. 68-71.
17. Inman, J.A., Danehy, P.M., Nowak, R.J., Alberfert, D.W., Fluorescence Imaging Study of Impinging Underexpanded Jets, 46th AIAA Aerospace Sciences Meeting and Exhibit, Reno, NV, 7-10 January, 2008.
18. Veser, A, Kuznetsov, M, Fast, G, Friedrich, A, Kotchourko, N, Stern, G, Schwall, M, Breitung, W, The structure and flame propagation regimes in turbulent hydrogen jets, International Journal of Hydrogen Energy, **36**, 2011, pp. 2351-2359
19. Xu, B.P. Zhang, H.P., Wen, J.X., Dembele, S., Karwatzke, J., Numerical study of a highly under-expanded H2 jet, 1st International Conference on Hydrogen Safety, 2005, Pisa, Italy.
20. Angers B., Hourri A., Benard P., Tessier P., Perrin J., Simulations of hydrogen releases from high pressure storage systems, WHEC 16, 2006, Lyon, France.
21. Swain, M.R., Codes and Standards Analysis, Annual Program Review Meeting of the Hydrogen, Fuel Cells and Infrastructure Program of the US Department of Energy, 2004.
22. Birch, A.D., Brown, D.R., Dodson, M.G. and Swaffield, F., The structure and concentration decay of high pressure jets of natural gas, Combustion Science and Technology, **36**, 1984, pp. 249-261.
23. Birch, A.D., Hughes, D.J. and Swaffield, F., Velocity Decay of High Pressure Jets, Combustion Science and Technology, **52**, 1987, pp. 161-171.
24. Ewan, B.C.R. and Moodie, K., Structure and Velocity Measurements in Underexpanded Jets, Combustion Science and Technology, **45**, 1986, pp. 275-288.
25. Schefer, R.W., Houf, W.G., Williams, T.C., Bourne, B., Colton, J., Characterization of high-pressure, underexpanded hydrogen-jet flames, International Journal of Hydrogen Energy, **32**, 2007, pp. 2081 – 2093.

26. Tchouvelev A., Hydrogen Implementing Agreement, Task 19 - Hydrogen Safety, Knowledge gaps in hydrogen safety - A white paper, 2008.
27. Han, S.H., Chang, D.J., Kim, J.S., Release characteristics of highly pressurized hydrogen through a small hole, International Journal of Hydrogen Energy, **38**, 2013, pp. 3503-3512.
28. El-Amin, M.F., Sun, S., Horizontal H2-air turbulent buoyant jet resulting from hydrogen leakage, International Journal of Hydrogen Energy, **37**, 2012, pp. 3949-3957.
29. Velikorodny A., Kudriakov S., Numerical study of the near-field of highly under-expanded turbulent gas jets, 4th International Conference on Hydrogen Safety, San Francisco, 2011, paper no. 169.
30. Papanikolaou, E., Baraldi, D., Kuznetsov, M., Venetsanos, A., Evaluation of notional nozzle approaches for CFD simulations of free-shear under-expanded hydrogen jets, International Journal of Hydrogen Energy, **37**, 2012, pp. 18563-18574.
31. Cheng, Z., Agranat, V.M., Tchouvelev, A.B., Houf, W, Zhubrin, S.V., PRD hydrogen release and dispersion, a comparison of CFD results obtained using ideal and real gas law properties, 1st International Conference on Hydrogen Safety, Pisa, Italy, 2005.
32. Chenoweth, D.R., Paolucci, S., Compressible flow of a two-phase fluid between finite vessels – II, Abel-Noble carrier gas, International Journal of Multiphase Flow, **18**, No. 5, 1992, pp.669-689.
33. Winters, W.S., TOPAZ – The transient one-dimensional pipe flow analyzer: an update on code improvements and increased capabilities, Technical report, SAND87-8225, Sandia National Laboratories, Livermore, CA, 1987.
34. Lemmon E.W., McLinden M O, Huber M L., REFPROP: reference fluid thermodynamic and transport properties. NIST standard reference database, **23**, No. 8.0, 2007.
35. Johnston, I.A., The Noble-Abel Equation of State: Thermodynamic Derivations for Ballistics Modelling, Australian Defence Science and Technology Organisation report DSTO TN 0670, 2005.
36. Pitts W.M. Effects of global density ratio on the centerline mixing behavior of axisymmetric turbulent jets. Experiments in Fluids **11**, 1991, pp. 125-134.
37. Keagy WR, Weller AE. A study of the freely expanding inhomogeneous jets. Proceedings of the Heat Transfer and Fluid Mechanics Institute, 1948-1950, **1-3**, 1948, pp. 89-98.
38. Fan, LH, Turbulent Buoyant Jets into Stratified and Flowing Ambient Fluids, Rep. No. KH-R-15, W. M. Keck Laboratory, California Institute of Technology, Pasadena, 1967.
39. Hoult, D.P., Fay, J. A., Forney, L.J., A Theory of Plume Rise Compared with Field Observations, Journal of Air Pollution Control Association, **19**, 1969, pp. 585-590.
40. Chen, C., Rodi, W., Vertical Turbulent buoyant jets, a review of experimental data. 1980, Pergamon Press, Oxford.
41. Molkov, V, Fundamentals of Hydrogen Safety Engineering, 2012, Ventus Publishing ApS, bookboon.com.
42. Mohamed, K., Paraschivoiu, M., Real gas simulation of hydrogen release from a high-pressure chamber, International Journal of Hydrogen Energy, **30**, No. 8, 2005, pp. 903-912.